Morphogenesis of a bundled tall building: biomimetic, structural and wind-energy design of a multi-core-outrigger system combined with diagrid

Francesco Laccone*, Alberto Casali[a], Marco Sodano[b], Maurizio Froli[c]

December 23, 2020

* (corresponding author)
Institute of Information Science and Technologies "Alessandro Faedo" (ISTI)
Italian National Research Council (CNR)
Via G. Moruzzi 1, 56124 Pisa, Italy
francesco.laccone@isti.cnr.it
tel. +39 050 621 2921
fax. +39 050 315 2810
Department of Energy, Systems, Territory and Construction Engineering
University of Pisa
Largo Lucio Lazzarino 1, 56122 Pisa, Italy
francesco.laccone@destec.unipi.it

[a] Bollinger + Grohmann Ingegneria Srl, Rome, Italy

[b] Pell Frischmann, London, UK

[c] Department of Energy, Systems, Territory and Construction Engineering, University of Pisa, Italy

Summary

Skyscrapers are among the most distinctive building types of the modern age. Since many resources are attributed to these buildings, their design should consider a proper performance-based construction economy and environmental sustainable development. This research introduces a new concept for a bundled tall building founded on the use of a multi-core-outrigger system, which is additionally enriched with diagrid structures. The concept is inspired by the bamboo plant and follows the biomimetic design principles for the structural organization, and performance-based criteria for optimizing the lateral stiffness and for shaping the cross section. Particularly, the incident wind speed is maximized to exploit Vertical Axis Wind Turbines (VAWT), which are located along the whole building height at the center of the bundled towers. The building morphogenesis is accomplished by a multi-step methodology that is fully developed in a parametric environment, and includes structural and computational fluid dynamic analyses. With the aim of validating the proposed concept, a case study of a 320 m-tall three-core building has been designed for the city of Pisa, Italy. The use of VAWTs results in an annual emissions reduction of about 10 $kgCO_2/m^2$.

Keywords

bamboo, diagrid, concrete core, outrigger, wind turbines, genetic algorithm, optimization, biomimetics

1   Introduction

Skyscrapers are among the most distinctive building types of the modern age. Their design mixes aesthetics needs to characterize the urban environment and performance-based requirements, which are related to their large-scale impact. Nowadays, they are moreover required to address a sustainable development, and so considering construction economy and environmental cost as key points since the earliest design phases [1].

Finding the form of a building is usually the most creative phase of the entire design work. Here, the technical considerations meet aesthetics and functional requirements in a continuous cycle of steps backward and forward until an optimal and balanced solution is reached. The aim of this paper is to introduce a new concept for bundled tall buildings and to present a methodology for the conceptual design inspired by the bamboo biomimetics. To mimic the structural efficiency and the functionally-graded material organization of the bamboo plant the present concept combines a multi-core-outrigger with diagrid. Since each single bundle is equipped with a core and a diagrid, a mega-frame behavior is obtained in which the lateral load is supported by shear and bending global forces acting on each tower. The design space among the bundles becomes thus available for hosting VAWTs, and consists in a building volume to sculpt in order to increase the energy efficiency.

The methodological framework for a tall building inspired by the outlined principles (Sec. 3) contains the conceptual biomimetic design in which the macro-scale parameters are defined, and the structural and wind-based strategies to size the main parts of the building. All the models are linked and developed in a parametric framework, and several tools are used, such as Finite Element (FE) structural and Computational Fluid Dynamics (CFD) analyses and generative algorithms. The effectiveness of the proposed concept and methodology is proved in Sec. 4, which reports on the morphogenesis of a case study of a 320 *m* tall building located in Pisa, Italy, which explores a three-bundles setting (a rendered view is in fig. 1 with a close-up on the VAWT, located in the inner space of the three bundled towers). The influence of the main design parameters on the building performances is evaluated and discussed. Eventually, the final case study design is validated (Sec. 5).

Figure 1: Render views of the proposed concept for a bundled tall building applied to a 320 *m*-tall case study in Pisa: overall view and detail of the vertical axis wind turbine.

2   Related work

The selection of a system tectonics and its preliminary design deeply affect the performance of the building. Indeed, large research efforts on tall buildings are spent on conceptual design and optimization procedures for structural systems [2, 3]. Although combined and designed in an unconventional way, the main structural components employed in this work, i.e. outrigger, core and diagrid, have been extensively investigated from this perspective individually.

Despite many variations and developments, the core system in tall buildings has been used since the late-nineteenth-century [4]. The reason of success lies in the easy integration of the walls with the vertical circulation, however their design is not trivial and depends on several architectural, structural, functional requirements. In the work [5], the wall layout complies with all these requirements and is optimized with respect to the weight. The problem of material consumption is a leading theme in this research area [6, 7]. If the bending moment increases, outrigger systems that activate exterior structures can relieve the core from overloading. The major challenge is to find the optimal outrigger placement for

improving the shear stiffness [8, 9, 10, 11].

Diagrid are exterior structures that wrap the building and are particularly efficient and robust in carry lateral loads and bending moments [12, 13]. Due to their aesthetic appeal and mechanic performance, preliminary design and optimization on diagrid systems constitute a fertile field of research [14, 15]. The works [16, 17, 18, 19, 20] introduce design strategies of sizing and optimization for different geometrical diagrid patterns.

Another research direction explores the shapes of a tall building. Here, a recent trend is to target an improvement of aerodynamic properties through shape modifications [21, 22, 23]. The purpose of this strategy might be to reduce wind forces or to take advantage of them as a sustainable energy source, i.e. by integrating wind turbines. In [24], a design technique is developed to optimize the stiffness for lateral drift design of tall asymmetric buildings involving coupled lateral-torsional motions. In [25], the authors introduce a corner aerodynamic optimization to reduce the wind load.

The opportunity of a building to produce energy from wind has been firstly explored in the Bahrain World Trade Center [26]. The 50-story building designed by Atkins is made of twin towers with tapered air-foiled cross section and integrates large diameter wind turbines. Three bridges link the towers at 60, 110 and 160 m, each holding a 29 m diameter horizontal axis wind turbine (HAWT). The shape is optimized to create a near equal wind regime on each turbine. They revealed lower performances than expected probably due to their fixed position, which entails losing wind energy coming from other directions. For this reason, although less efficient, the vertical axis wind turbines (VAWT) appeared to be more appropriated for high-rise building implementation. The Pearl River Tower in Guangzhou (China) designed by SOM is 309 m tall with an aspect ratio of 1:8, and embeds VAWTs [27]. The building has a rectangular plan, and it is concave on the southern side to collect the wind from the prevailing direction, and convex on the northern side. 2x5 meters VAWTs are located within four openings, two per level. This particular geometry amplifies the wind speed (around $4.3m/s$ at 50 m) by a factor $2 - 2.5$. The energy-production capacity is lower if compared to the Bahrain tower because of the smaller turbine dimensions, although the daily usage percentage is remarkably larger.

Innovative concepts and developments are introduced from the so-called "outside-the-box" design strategies. One of them is the biomimetic approach, which represents a new interesting way to investigate a complex design space. Hence, the application of a bamboo-based analogy has proven to be very promising. The idea to take advantage of the bamboo proportions and map them into structural systems is included in at least two significant cases. The Taipei 101, the 502 m tall skyscraper designed by C.Y. Lee & Partners, is a particularly interesting example of imitation of a bamboo stem. The level of natural replication is mostly aesthetic, except for the adoption of stiffening rings to mimic each bamboo node [28]. SOM's tower at the China World Trade Center, contrarily, is based on an extensive bamboo mimicry [29]. The concept for this super-tall building is established on the collaboration between a mega-brace outer structural frame, entirely proportioned according to the mathematical model that describes the relation between the bamboo's internode lengths, diameters and nodes, and an inner ductile moment-resisting frame, connected to the outer frame at each node.

3 Design method

The methodological design scheme proposed in this work is illustrated in fig. 2. The morphogenesis represents the central point of the scheme and is the process in which the building is formed and all its main components are spatially arranged. This process is the synthesis of a two-phase method, which can be possibly iterative: biomimetic design (Sec. 3.1) and performance-based design (Sec. 3.2).

The biomimetic design is a set of four consequential steps that aims at grasping a specific biological structure (a bamboo plant and its growth pattern) and transferring it into a comparable technological product (a tall building) in order to improve its quality or to solve a specific technical question. The performance-based design is targeted on three design scales. In particular, firstly the bamboo growth model is applied on a beam model, where the design space of macro-scale parameters is explored and all solutions are compared in stiffness (Sec. 3.2.1). Secondly, the cross section of the building is shaped with the aim of maximizing the wind velocity that is incident on the wind turbines (Sec. 3.2.2). Thirdly, the structure is sized and optimized with respect to lateral deformation (Sec. 3.2.3).

The validation of this method has been performed on a case study of a tri-core tall building. The building is 320m-tall and has been designed to be located in Pisa, Italy. The first part of the validation consists in the allocation of functions within the building to be compliant with architectural needs and safety. The second part is the structural analysis of the building. The third part is the energetic analysis that focuses on a 3D CFD analysis and the estimation of energy production from wind turbines.
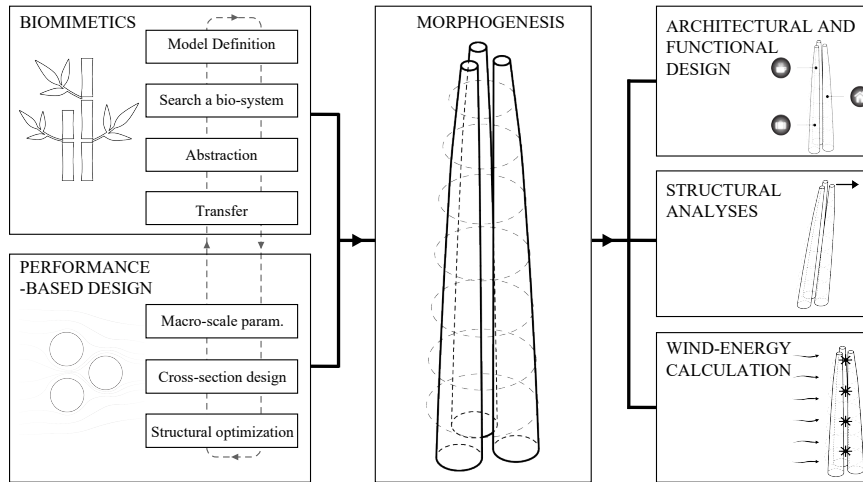
Figure 2: Methodological design scheme adopted in this work.

3.1 Biomimetic conceptual design

The theoretical framework of this part of the methodology is provided by the Technology Pull method, a top-down approach for biomimetics of buildings [30]. This approach starts with the problem identification and the selection of a natural model. Afterwards, the model is abstracted and transferred to the technical application. The building peculiarities considered in this phase are wind-related: the building has to face lateral wind-induced load and simultaneously it requires wind as a source of energy. The biomimetics assumes as objectives:

- To obtain a good stiffness of the building without increasing area and mass of the core;

- To optimize the horizontal displacement due to lateral forces;

- To maximize wind speed on the VAWTs.

The main conceptual step in a biomimetic design methodology is the identification of a link between the stated objectives (building requirements) and the characteristics of a biological system, which is supposed to be inherently efficient. In the present case, this is represented by a bamboo stalk. Its structure and geometric proportions makes it able to respond effectively and efficiently to lateral loads [29]. The culm, which represents the trunk of the plant, has a hollow circular section that is tapered from the base towards the top. The culm presents nodes, in which it is transversely stiffened at varying heights by diaphragms. The culm portion between two nodes is a cylindrical shell named internode. Some species can reach extraordinary heights of $35 - 40$ m, the thickness of the culm can reach up to 3 cm, its diameter up to 30 cm.

Bamboo is made up of long cellulose fibers embedded in a wooden matrix, and can be defined as a functionally-graded material, which means that its material structure gradually varies within the volume. This feature develops either at the micro-scale, since the amount of fibers varies on the cross section of the culm; and at the macro-scale, since diameter, thickness and length of the internodes are also graded in height. Bamboo is one of the natural systems whose life-cycle self-organization identifies a so-called growth pattern. Its formation reveals a unique feature: the future structure of the culms (namely the internodes and the nodes) is already known and preserve the same features since the buds of the rhizomes are growing underground, before they become bamboo shoots and emerge from the ground. For this reason the growth can be mathematically described.

At macro-scale level, the bamboo growth pattern can be abstracted using a quadratic formulation by Janssen [31], which is calibrated on averaged properties of fifteen different bamboo species. The nodes are not evenly spaced, but they are closer in the proximity of the base and towards the top. This feature prevents the instability of the culm walls with respect to gravitational and lateral loads. Moreover, the culm thickness and diameter vary along the height: the cross section is greater at the base and thins out towards to top. In this formulation eq. 1-3 the internode length L_i, the internode

diameter D_i and the wall thickness t_i can be expressed as function of the internode number n_i.

$$\begin{cases} L_{i,bot} = 25.13 + 4.8080\,n_i + 0.0774\,n_i^2 \\ D_{i,bot} = 97.75 - 0.2120\,n_i + 0.0160\,n_i^2 \end{cases} \qquad n_i \le 0.4 \qquad (1)$$

$$\begin{cases} L_{i,top} = 178.84 - 2.3927\,n_i + 0.0068\,n_i^2 \\ D_{i,top} = 157.60 - 2.8680\,n_i + 0.0130\,n_i^2 \end{cases} \qquad n_i > 0.4 \qquad (2)$$

$$t_i = 35 + 0.0181(n_i - 35)^{1.90} \qquad (3)$$

The functions plots are represented in fig. 3, where for sake of simplicity all values are normalized. The internode number is set as 0 at the level of the bottom internode, and 1 at the level of the highest one; similarly the internode length and diameter are normalized on the greatest length and diameter respectively.
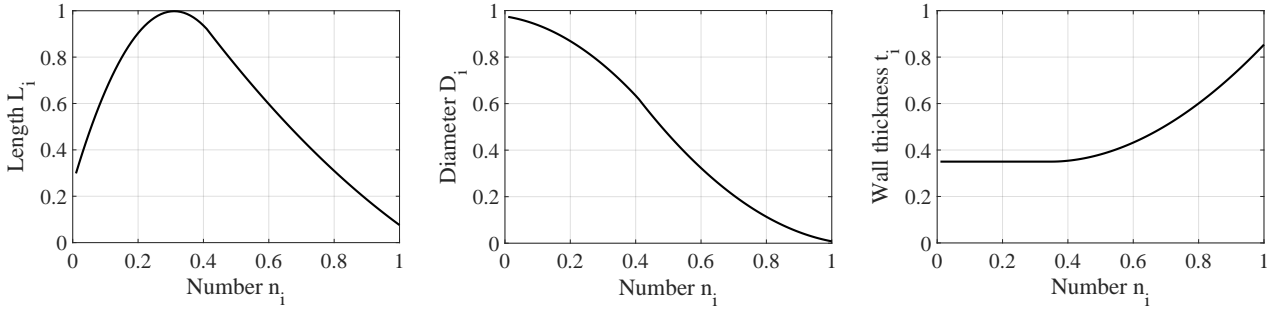

Figure 3: Function plots of the bamboo growth pattern as per eqs. 1-3. The parameter t_i is reported for completeness but has not been used in the present methodology.

To enable the model transfer into the design domain the following principles are adopted.

- Outriggers are located at each bamboo node to reduce lateral displacement (fig. 4a).

- A nonlinear tapered profile in accordance with the growth pattern is adopted (fig. 4b), with the effect of increasing the resistance the tilting moment caused by lateral loads.

- The load-bearing elements are located in a centrifugal arrangement to provide bending resistance and optimal use of the material (fig. 4c).

The proportion of the building and the position of the outriggers are defined by the growth pattern. The cross section is segmented to obtain bundled towers, each equipped with an individual core and a diagrid. The towers are transversely connected by outriggers as shown in fig. 5a. The subdivision into bundle towers reduces floor spans and so their mass, which is significantly beneficial from an earthquake engineering point of view, and reduces the surface exposed to wind, being the wind load the strongest external force acting on the building (fig. 6b). The outriggers are paramount for activating the bending capacity of the building section by means of compressive and tensile forces of the single towers. The whole building expresses the concept of robustness at different levels. The bundled towers are functionally and structurally independent but connected at the outriggers, which means that the building can compensate damages and out-of-service areas relying on the support and alternative paths provided by the undamaged ones. Therefore, the outrigger also plays a fundamental functional role of connector between the towers. This feature is useful in emergency scenarios, i.e. it creating multiple exits and escape routes in the event of fire, but also creates a meeting place or gardens for the daily use of the building (fig. 6c). On the other hand, each tower that is equipped with both a concrete core and a diagrid is itself redundant.
The role of main lateral system is played by the diagrid that additionally provides bending resistance in combination with the outrigger. Instead, gravitational load are mainly carried out by the core. The concrete core is designed to meet architectural and functional goals of creating a central hub, which extends from the bottom to the top of the towers and leave as much as possible free space on each floor plan. Due to the tapered shape of the building, the bundled cores are also consequently tapered to preserve the alignment of the inner core walls.
To induce a Venturi's effect in the space between the bundled towers where VAWTs are installed (fig. 5b) the tower inner space is shaped by wind. Eventually, the design solution stands between an external bound, which is defined by
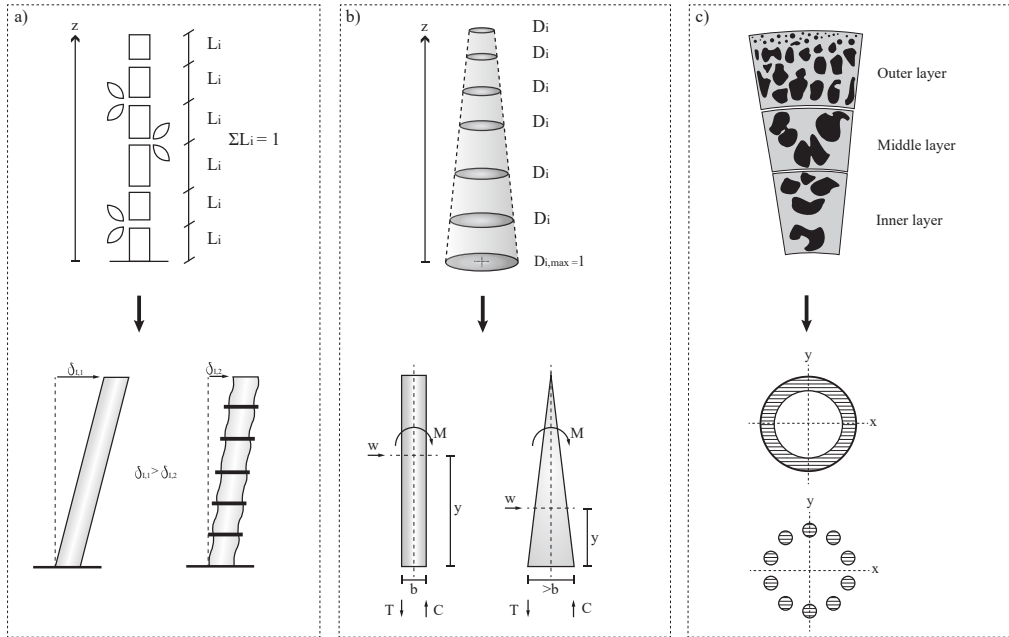
Figure 4: Mechanics of bamboo transferred into the design of a tall building: (a) outrigger placement; (b) tapering; (c) bundle.

the macro-scale biomimetic parameters, and an internal bound, defined by the empty space that is needed for developing wind flow features to push the VAWTs and generate energy. The conceptual design is managed with a parametric model developed in Rhinoceros and Grasshopper [32] in which eq. 1-3 have been transferred. Hence, the sum of the internodes length becomes the total height of the building, while the diameter is converted into the building outer diameter.
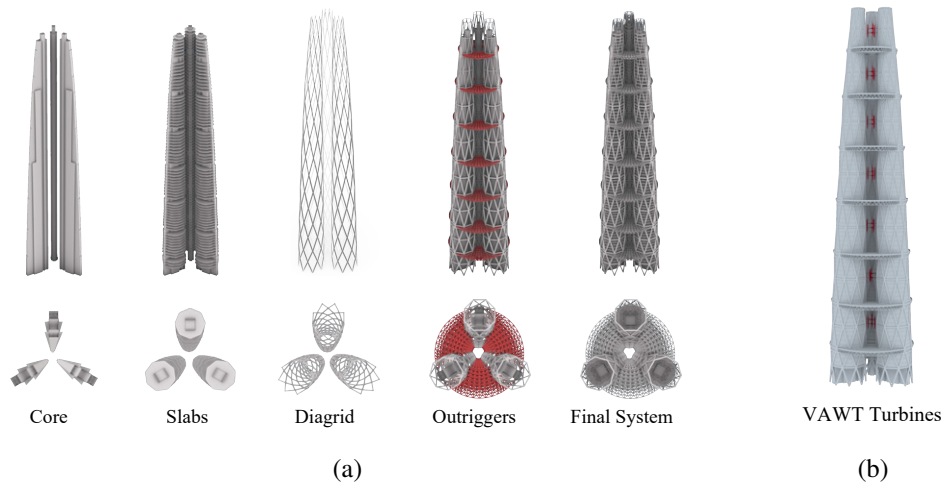

Figure 5: Structural system introduced in the present concept (a), and VAWT building integration (b). The figure illustrates the design solution adopted in the case study.

3.2 Performance-based design

3.2.1 Macro-scale parameters investigation

Two groups of simplified parametric models are employed to understand the sensitivity of the abstracted macro-scale parameters on the statics of the building. The lateral stiffness of the building is the unique guiding criterion, so vertical loads are neglected and wind load is considered as horizontal load. The first group of models is built at the building
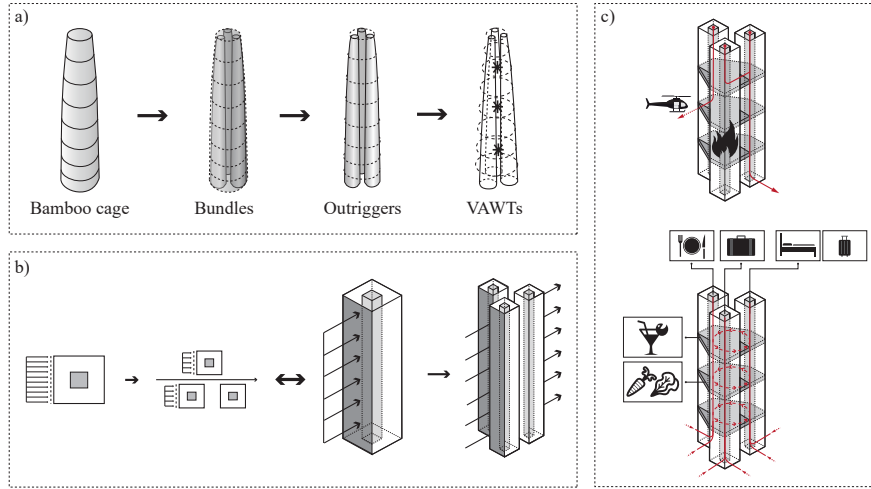
6

Figure 6: Mechanics of bamboo transferred into the design of a tall building: (a) shaping of the boundle geometry; (b) wind load effect on bundles; (c) functional design.

element scale and is intended to evaluate the shear stiffness of a hollow tube with rigid diaphragms. The second group includes the bundled towers as a further refinement of the cross section. To quantify the practical advantages of adopting a bamboo biomimetic approach, these systems are compared with their 'regular' competitors having comparable height and volume, such as a building with equally-spaced outriggers and a non-tapered building.

A limit of the bamboo growth model is that the upper internodes are characterized by an excessive reduction of lengths and diameters. This effect is beneficial from a structural viewpoint because the tip is stiff and less sensitive to drift; on the other hand, it is negative from and architectural and functional viewpoint because the number of bulky diaphragms reduces the utilizable volume and increases costs. The adopted solution consists in imposing a limit value in the normalized number of nodes to exclude values higher than this limit. The functions are linearly re-normalized as per fig. 7. A drawback is that this limit imposed in the original plot constitutes another design parameter to explore.
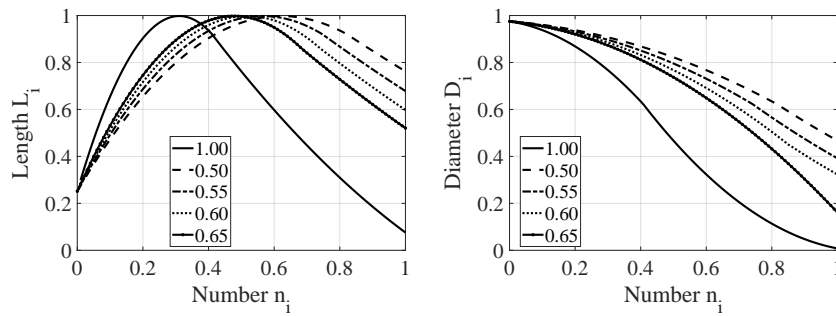

Figure 7: Rescaled bamboo functions with different model limits (0.50, 0.55, 0.60, 0.65, 1.00).

Input data to generate the models are the number of internodes, the total height of the building, the aspect ratio, the bamboo model limit. As a result, a series of diameters obtained as per eqs. 1-2 defines coaxial circles at different height of the building. The surface through the circles provides the outer bound of the building as shown in fig. 8.

The element-scale model is linked to macro-scale parameters and adopts the tapered shape provided by the outer bound with rigid diaphragms for each node. This model results in a shear-type cantilever. The bundled model includes the bundle geometry as a series of tapered hollow cylinders inscribed in the outer circle bound (fig. 8). In order to take into account the space occupied by the wind turbines, a void internal cylinder with a constant diameter throughout the building height is considered non-design space D_{void} in fig. 8. For this latter group of models both shear-type and bending behavior is investigated.

As the aim of these analyses is to provide general understanding of the lateral response of a bamboo-based design, the values of the drifts are to be regarded not in the absolute terms and may be used to make comparison. Linear elastic analyses are adopted, and a cross section with Young's modulus $E = 210\ GPa$ and thickness $0.3\ m$. Having load-bearing

material only along the circles, these models well simulate outrigger buildings in which the stiffness of the diagrid is prevailing on the core.
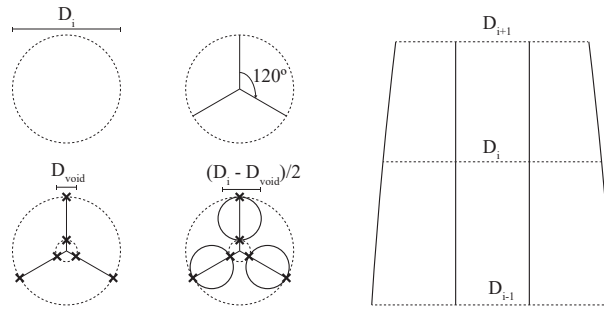

Figure 8: Geometry generation of the bundled building within the bamboo model design space.

3.2.2 Cross section design

Once the macro-scale parameters are fixed, the cross section can be further sculptured through fluid-dynamics in order to develop a plan shape which maximizes the wind speed inside of the building through the Venturi's effect. The adopted approach considers different shapes of the bundled towers and observes their effect on the air flow by means of a 2D CFD analysis. The mean velocity in the inner area is the target parameter to maximize. The wind turbines are designed to be placed at the average height between each outrigger with the exception of the first internode, in which the wind speed is low.

The simulation runs in a square domain whose edge is three times the diameter of the building. The explored shape options are included in the circumscribed circle at the specific internode (fig. 9). For each case, two shape modifications are explored. The first concerns the dimension of the void, namely its inner radius R_{void} (fig. 9), which defines the void internal cylinder between the towers. The second is on the cross section of each bundle tower, which is assumed to be as:

- a circular shape, in which the outer circle knot is tangent to the internode circle.

- a triangular shape, with a curved outer edge whose radius is half of the internode diameter. The fillet radius R_{fill} (fig. 9) of all vertices has represented an additional varying parameter.

- a triangular shape that is similar to the previous but the additional varying parameter is the fillet radius R_{fill} (fig. 9) of the only outer vertices. This case has been intended to explore the effect of a zero-fillet radius in the inner vertex.

The CFD analyses have been conduced within the software OpenFOAM [33], while the geometries and the setting up of each model has been obtained with Butterfly [34], a python-based Grasshopper plugin.

The target average velocity has been evaluated through integration of the velocity vectors over the mesh cells contained into the inner circle. This inner circle represents the influence area of a VAWT. The optimal shape is selected as the case with the highest average speed according to considered flow directions.
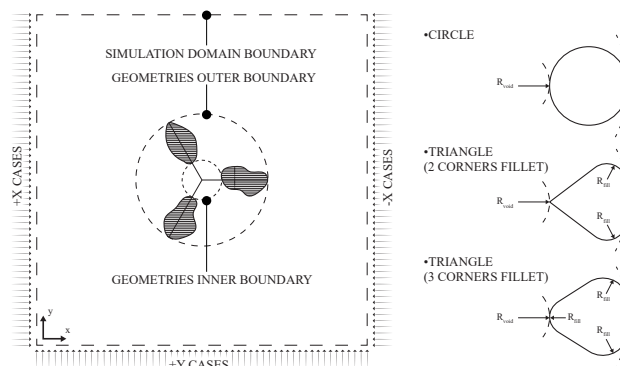

Figure 9: 2D CFD analysis method: analysis domain and explored shape options

3.2.3 Structural sizing and diagrid optimization

The unusual combination of diagrid, core and outrigger provided by the present concept makes the structural design a complex task. Because of their triangulated configuration, diagonal members in diagrid systems can carry both gravitational and lateral forces, however they are expected to be particularly effective in minimizing shear deformation since they carry shear by axial forces. The bending behavior is expected to be governed by both diagrid and outrigger, but also the bundling plays a relevant role in producing a mega-frame behavior that activates the cores. The strategy for structural sizing here adopted considers redundant and safe assumptions and state-of-the-art methods. In particular, the concrete core has been designed on a strength criterion to support the entire gravitational load and the lateral wind-induced shear force. This phase considers also constraints from the shape (i.e. tapering) and from the vertical circulation. The steel diagrid has been designed with the stiffness-based methodology by Moon et al. [35], considering the wind-induced shear and the bending moment acting on a single tower.

To avoid oversizing problems the diagrid cross sections are further controlled and computationally optimized. The optimization process has been managed by the tool Galapagos, a genetic solver integrated in the Grasshopper environment. As single-objective evolutionary solver, it requires two inputs: as series of variables cross-sections diameters, and as fitness number the drift. The solver progressively modifies the model in search of a solution.

3.3 Design validation

The architectural and functional design is part of an holistic vision of the building and not intended a mere consequence of the structural design. Since only few parameters have been explicitly designed and managed within the precious steps, all architectural and functional requirements, i.e. related to vertical circulation, safety and allocation of functions, need to be verified in a subsequent phase, once almost all structural and wind-related parameters have been defined. It is recommended to cross-check the concrete core adequacy to perform as hub of vertical circulation and possibly to inform the structural sizing in Sec. 3.2.3. The optimized cross-section found as per Sec.3.2.3 are plugged-in in a new model that is generated in the Grasshopper parametric environment. Using the plugin Geometry Gym [36], the structural model is directly generated and exported in the SAP2000 environment [37] for the FEM analysis. Additionally, in this model the outriggers as spatial trusses have been explicitly included, and the ideal rigid plane simplification employed in the previous models has been removed.

The wind energy production has been evaluated through statistical methods and input data provided by the European Wind Atlas [38]. The wind rose has been subdivided into 12 sectors, and a Weibull's function has been specialized for each wind direction. Using the vertical wind speed profiles as boundary conditions, 3D CFD analyses have been performed for all the twelve wind directions. Due to the high computational cost, these analyses have been developed within the SimScale platform [39], a cloud-based CAE which includes also a computational fluid dynamics tool. The main purpose is to evaluate the effective building-induced velocity gain at the level of each turbine. This is obtained by the ratio between the inlet velocity and the average velocity inside the VAWT volume of influence. Hence, given the probability density of each velocity, the building-induced velocity gain at every height and the swept area of each turbine, it has been possible to calculate the wind power amount at the various height and directions. The annual energetic production can be evaluated by multiplying these values by the turbine power coefficients and integrating them on the period of one year. The VAWT size has been chosen to be the greatest possible according to the available design space.

4 Case-study morphogenesis

Input data adopted in the case study morphogenesis are included in Tab. 1 and are discussed in the following sections. The 320 m building adopts three bundled towers, eight internodes and seven VAWTs.

4.1 Parametric analysis on macro-scale parameters

The parametric model explores as macro-scale parameters four different height values H (200 m, 260 m, 320 m, 380 m), four aspect ratios D/H (1:3, 1:4, 1:5, 1:6), four bamboo model limits (0.50, 0.55, 0.60, 0.65). Due to the absence of a specific calibration of the cross section, these results should only be regarded in relative terms and not for achieving directly the correct stiffness of the system. The results are marked with the acronyms shown in fig. 10, in which is included a schematic representation of all investigated models. In order to decouple the main sensitivities different structural schemes are adopted.

Table 1: Summary of the case study project data

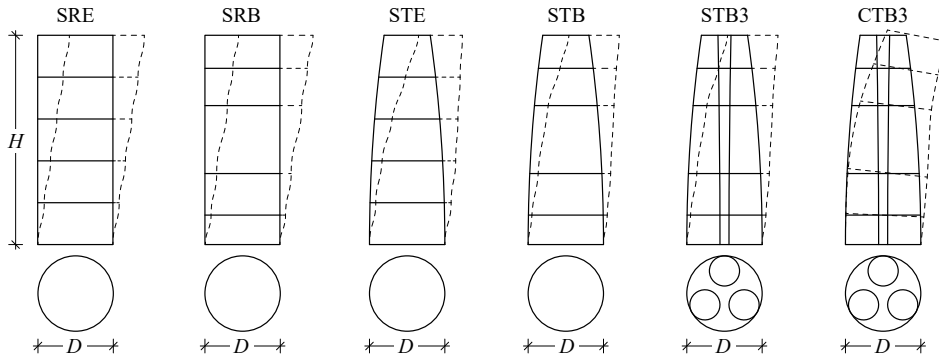|	Project data	Unit
Location	Pisa, Italy (elevation: 4 m)	
Type	mixed-use	
Floors number	77	
Total available area	34400	m^2
Building height	320	m
Circumscribed base diameter	80	m
Circumscribed tip diameter	37.3	m
Aspect Ratio	1:4	
Bamboo model limit	0.55	
Internodes number	8	
Outrigger number	7	
Towers number	3	
Installed VAWTs	7	

Figure 10: Schematics of the models investigated within the parametric analysis. The first letter in the acronym points at the mechanics (Shear type or Cantilever), the second at the building shape (Regular or Tapered), the third at the position of the outriggers (Equally-spaced or arranged as per the Bamboo growth model), lastly the number 3 is added for the models that uses a three-bundle setting.

4.1.1 Effect of macro-scale parameters and outrigger spacing

To quantify the sensitivity of the model to macro-scale parameters, such as number of internodes, aspect ratio, height, bamboo model limit, and to evaluate the effect of the outriggers spacing the lateral response of the models SRE and SRB is compared. Both models have single-core and constant circular hollow cross section, but in the SRE the outriggers are equally spaced, while in the SRB they follow the growth pattern. Since at the element scale the bending stiffness is not affected by the outrigger spacing nor by all other parameters, only the shear stiffness is investigated. A shear-type cantilever model is adopted. The plots in fig. 11 report the tip drifts Δ versus aspect ratio, growth model limit and internodes number. To enable easier comparisons all drifts are divided by the height H. From all plots it can be observed that the SRB models perform better than their SRE counterparts. By adopting the SRB the drift is beneficially reduced on average by a quantity that is slightly above the 50%. In absolute terms the bamboo spacing is particularly convenient in the case of tall buildings and low number of outriggers.

It is interesting to note that all models regardless of the outrigger positioning show similar sensitivity to macro-scale parameters. In particular, an increase of the internodes number (so of the outriggers number) results as expected a good strategy to increase the lateral stiffness as long as the building is slender (aspect ratio smaller than 1:5) or taller (fig. 11a). If the number of internodes becomes larger than 8 the benefit lowers.

The bamboo model limit has almost null influence on the drift as it can be observed in fig. 11b, in which all curves cluster in two groups. This effect is recurring for all aspect ratios, although fig. 11b reports only the case of 1:5, and can be also observed on fig. 11c since the drift is mostly constant with respect to the model limit. The bamboo model limit influences both the internode lengths and the tapered shape. However, since the models adopted a constant cross section it is possible to conclude that the shear stiffness is faintly affected by the internode lengths.

Fig. 12a reports shear-only lateral deformations comparison between SRB model with 0.55 model limit and the related

SRE model. Similarly to the real bamboo plant, it emerges that the bamboo-spaced outriggers provide comparatively a larger stiffness at the tip and at the base. Observing the markers in the plots it could be noted that the required shifting of the outrigger from the SRE to the SRB is quite small if compared with the benefit it produces. Taking advantage of this alteration provides a deformed shape which can be only obtained by increasing the number of equally-spaced nodes. Favorably, this alteration is far from affecting the aesthetics of the building.
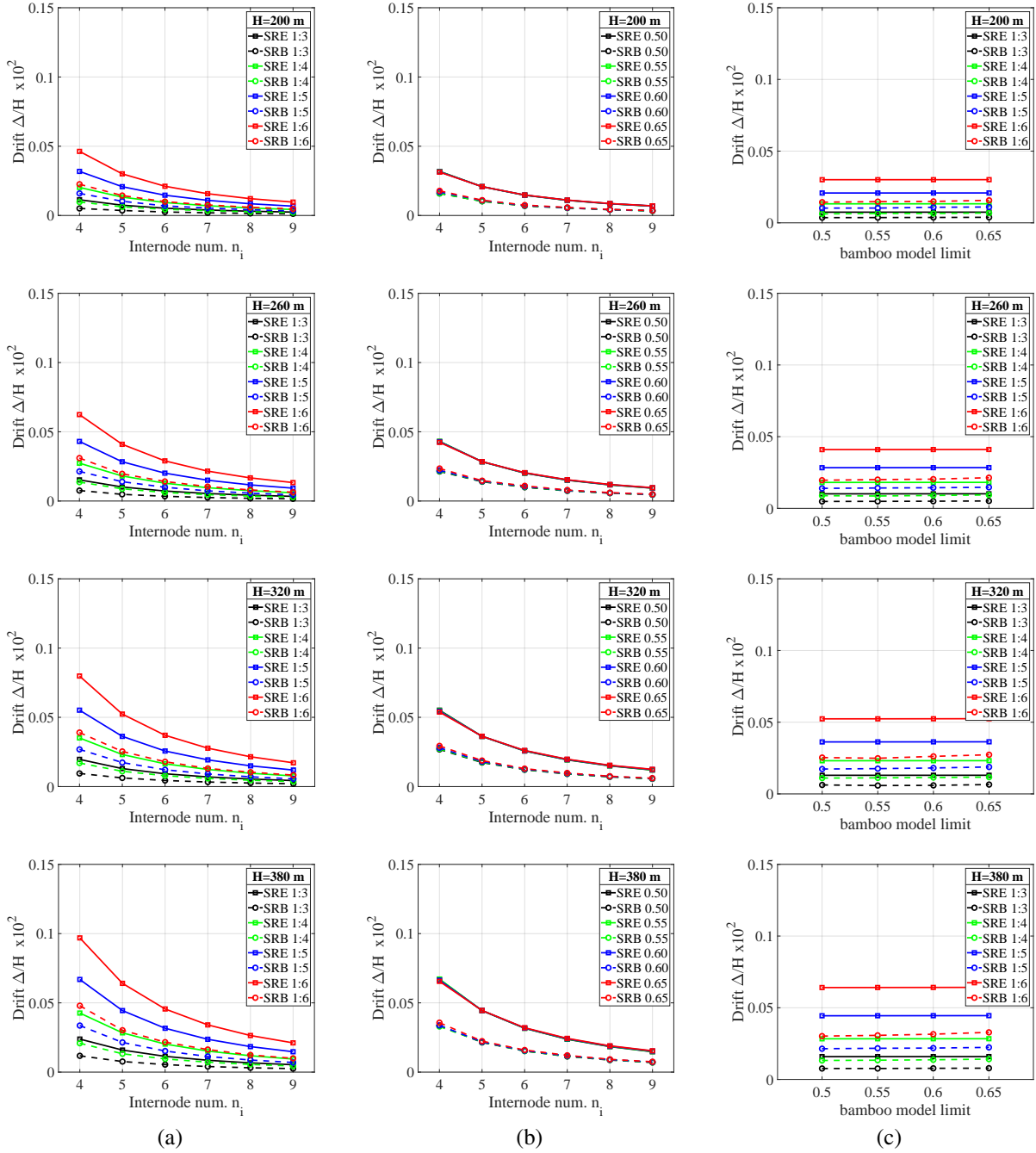

Figure 11: Parametric investigation on macro-scale parameters and outrigger spacing: (a) aspect ratio (growth model limit set to 0.5); (b) growth model limit (aspect ratio set to 1:5); (c) aspect ratio (number of nodes set to 6). The rows denote different heights.

4.1.2 Tapering effect

To quantify the influence of the bamboo tapering at the element scale two shear-type models are compared: the regular SRB and the tapered STB. The SRB is a model that has the same volume of the STB and a base diameter that is constant throughout the height. Their counterparts with equally-spaced internodes SRE and STE are also included. Fig. 12b represents the tip displacement for all models for varying numbers of internodes. Although the tapered and regular models could be considered similar from a urban impact viewpoint, it is worth noting that the lateral load is proportional to the area, so the SRB model is subject to a higher load. The main difference of drifts can be thus justified. Overall, for a constant volume of the building the tapering brings a minor benefit on shear deformability, but remarkably even for the tapered shape the bamboo spacing of the outriggers confirms as a beneficial strategy. Moreover, as the aspect ratio is kept constant, the drift lowers if the height decreases, similarly to the regular building. The higher is the building the higher is its drift sensitivity to the number of internodes.

4.1.3 Bundling effect

Adopting a bundled setting in place of a single core produces two main effects of decreasing the shear stiffness and of changing the bending behavior from a simple cantilever to a mega-frame cantilever. To provide quantitative information on these two points, two groups of models with same bending stiffness at all levels are compared: the STB model, which has been discussed in the previous section and as representative of the single-core geometry, and two bundled models STB3 and CTB3. The STB3 is a shear-type model that considers three in-parallel bundles. The CTB3 has both shear and bending deformability. All the models have same lateral load. For sake of conciseness, only the case of $H = 320\ m$ with aspect ratio of 1:4 has been shown in figs. 13-14. This is a representative output for all other cases, which manifest the same trend, and will be also the reference geometry for the case study (Sec. 4).

By discussing the shear stiffness of the two systems it can be noted that even if they present the same deformed shape the STB3 lateral deformation is at least one order of magnitude larger than STB (fig. 13). What has been previously said on the single-core model is still valid in relative terms, but the effects have be considered as intensified. Indeed, it could be stated that the number of internodes increases the stiffness but this effect is lowers for internodes larger than 7 or 8, as for the single-core. Conversely, it emerges that while for the single-core models the bamboo model limit has almost null effect, for the CTB3 it produces slightly different deformed shapes. Moreover, the higher the bamboo limit the lower the stiffness. This dependence is visible for a low number of internodes while it attenuates if this number increases.

Due to the high shear stiffness of the single-core model, it is meaningless to compare the deformed shapes of the single-core cantilever and the CTB3. In fact, the only comparable feature will result in the amplitude of the tip displacement, since both systems are calibrated to have the same inertia. Instead, it is better to focus on the deformed shape of the CTB3 models. It is noted that the bending stiffness increases with the number of internodes. So, adopting more outriggers is a sound strategy to increase both the shear and the bending stiffness. Another effect to note is the dependency of the bending stiffness on the bamboo limit. In particular, deformed shapes with a low bamboo model limit (such as 0.50 or 0.55) are stiffer up to 0.7 H while become more deformable beyond this limit. This particular shape evidences for the first time the effect of the diameters variation associated with bamboo model limits. The CTB3 is notably effective in highlighting this dependency on the nonlinear tapering function, which brings changing of diameters and lengths of the internodes. The shifting observed on the STB3 curves due to the bamboo model limit could be regarded as a decoupled effect of the only internode length sensitivity from the CTB3 curves.

The rotations on CTB3 models are shown in fig. 14. To improve the readability of the plot only the limit curves of 0.50 and 0.65 bamboo limits are reported. The absolute rotations (fig. 14a) are in all cases similar up to 0.3 H while they cluster for increasing heights in two groups. The curves of each group do not manifest same tendency due to different nonlinear tapering functions associated with the single tower. However, at 0.6 H the rotation reaches its maximum and it remains approximately constant. If instead of the rotation, the discussion is moved to the vertical displacement caused by that rotation it can be observed that the clustering is less evident and most importantly the displacement lowers from 0.6 H up. This trend is due to the diameter reduction of the circumscribed circle.

4.1.4 Discussion on parametric analysis

The single-core models neglect the bending stiffness and present several limitations. However, they have the advantage of being simple to be computed by hand calculations. Indeed, they can support the designer in the early phases and permit to well observe the effect of the aspect ratio and of the bamboo spacing. Even though in general it is not possible to explore a wide height range, a taller building such as the 320 or 380 m in the examples has more benefits from the adoption of the present methodology, as well as a high slenderness for a given height. An increase of internode numbers, which means to adopt more outriggers, leads to a stiffer response in absolute terms. But given a number of internodes, altering their
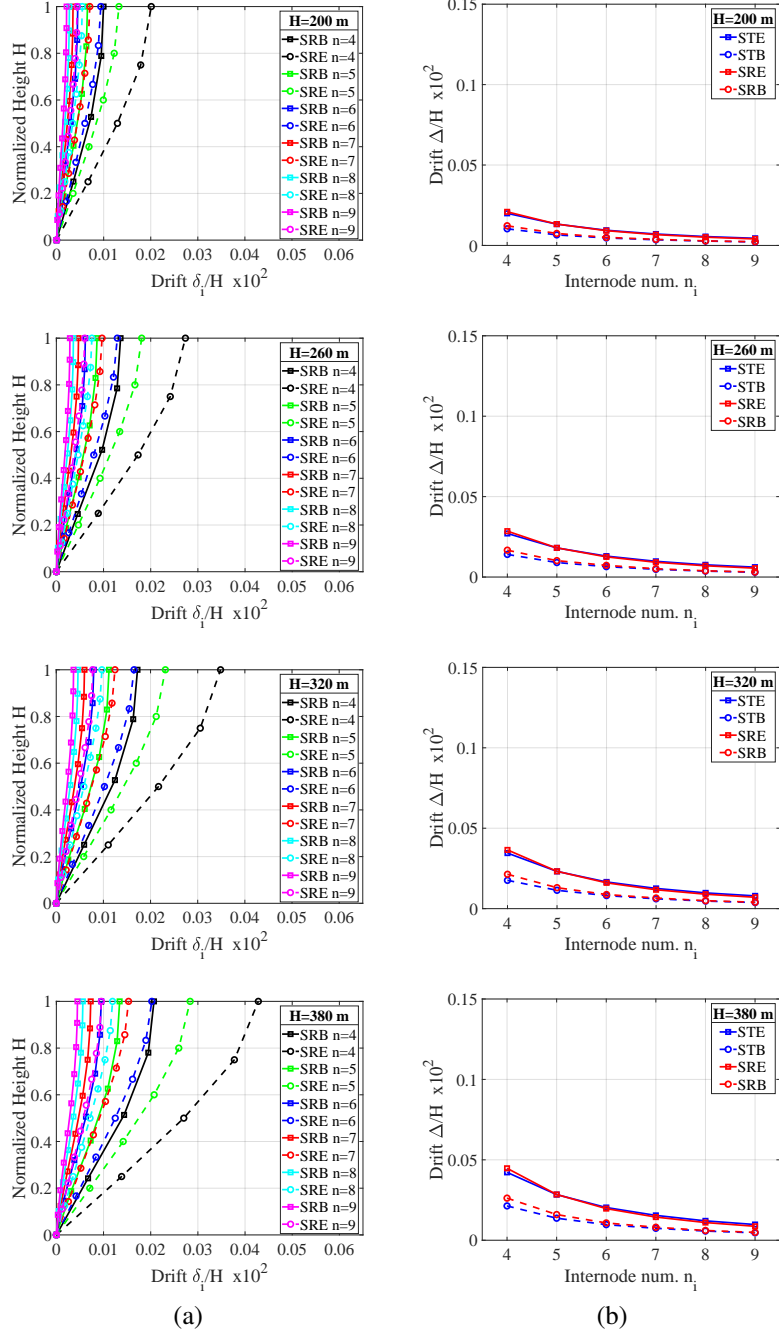
Figure 12: Parametric investigation on macro-scale parameters and outrigger spacing: (a) qualitative shear-only deformed shape comparison (aspect ratio set on 1:4, bamboo model limit to 0.55 for the SRB); (b) tapering effect (aspect ratio set to 1:4, bamboo model limit to 0.60). The rows denote different heights.

spacing according to the bamboo pattern brings to a shear stiffness that can be achieved only in an equally-spaced setting with at least one additional node. This characteristics is preserved also for the bending stiffness.

The tapering function is governed by the bamboo model limit. To analyze exhaustively this feature a multi core model is required because it is able to interpret modifications on both shear and bending behavior. The final deformed shape of the building results akin to a mega shear-type column with an inflection point, whose position is around 0.7 H for the 320 m tall example. And the higher is the bamboo model limit the larger is the curvature of the shape. So it appears more suitable to select as limit 0.50 or 0.55.

Lastly, it is worth mention that by adopting a bundle setting there is a change of stress on the cross section. The bundled
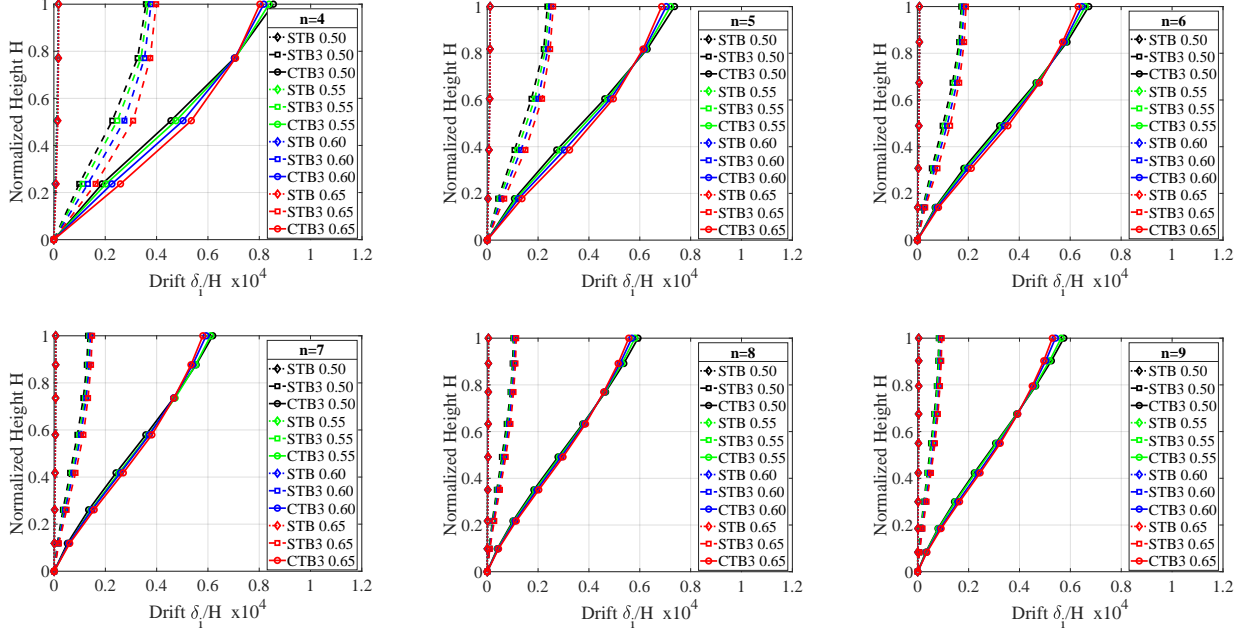
13

Figure 13: Bundling effect for the $H = 320\,m$ model (aspect ratio set to 1:4).
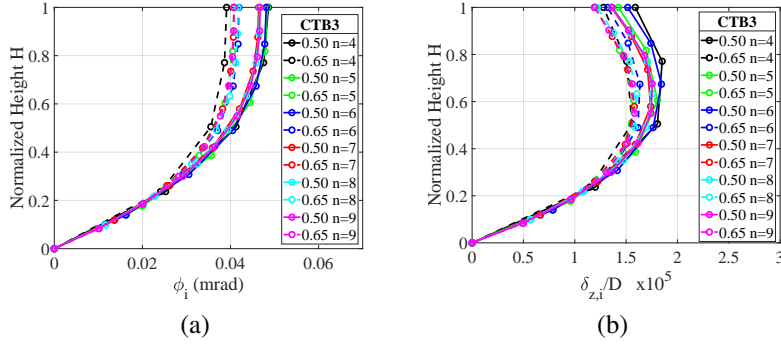

Figure 14: Bundling effect for the $H = 320\,m$ model (aspect ratio set to 1:4, bamboo model limit set to 0.50 and 0.65): (a) rotations; (b) maximum vertical displacement.

cross section has polar symmetry, and global bending force activates tension and compression in the single bundle. Conversely, the single-core bending stress varies from positive to negative values throughout the section. Moreover, if both sections have same bending stiffness, the shear stiffness of the bundled setting is lower than the single core. It should be recalled that all the results of the parametric analyses are produced with simplified models and consider a combination of hollow tubes with lateral loading. They are intended to be used as a guide to select a tentative combination of macro-scale parameters and strategies, which need to be validated in a subsequent phase.

4.2   Parametric analysis on cross section shaping

The cross section design has been established at the level of the lowest wind turbine, located at $53\,m$. Each case has been tested for varying radii of the internal empty circle R_{void} ($7.5\,m$, $10\,m$ and $12.5\,m$), and values of 0, 5, and $10\,m$ are explored as filleting radius. Values greater than $10\,m$ transform the triangles into the circles. By considering all combinations of fillet and inner radius, totally 24 configurations have been investigated along three wind directions ($\pm$X and $+$Y).

The Reynolds Averaged Navier–Stokes Equations (RANS) CFD analyses have been based on $k - \omega$ turbulence model, with an expected inlet velocity of $10\,m/s$ for each case. The mesh is uniformly sized to $50x50\,cm$ quads, with refinements of $25x25\,cm$ close to the towers. The highest velocity up to $12\,m/s$ has been provided by the 3-corners filleted triangle

shape with the lowest value of $R_{void} = 7.5\ m$, retrieving an average velocity of 21.81 m/s among the favorable flow direction +X. For each shape, as the R_{void} value increase the velocity amplification decrease, which is in line with the expectations. Concerning the two triangle shapes, the chamfered corner affect negatively the flow, causing a vortex that lowers the velocity. Vortices are also discouraged since they can cause unwanted vibration in the turbine and reduction of power generation.

Considering the most unfavorable direction -X reported in fig. 15, the two triangle shapes are unable to recollect part of the flow deviated by obstructing tower, instead the circular bundles are able to achieve this result. In particular, when the $R_{void} = 7.5\ m$, they can not only to recollect part of the flow, but also increase the velocity of 2%. Eventually, the case with circle bundles and $R_{void} = 7.5\ m$ has been selected because it performs better on average and there is always an increase of velocity. In this configuration, the velocity increases of the 12% for the +X case, of the 2% in the -X case, and the 19% in the +Y case.

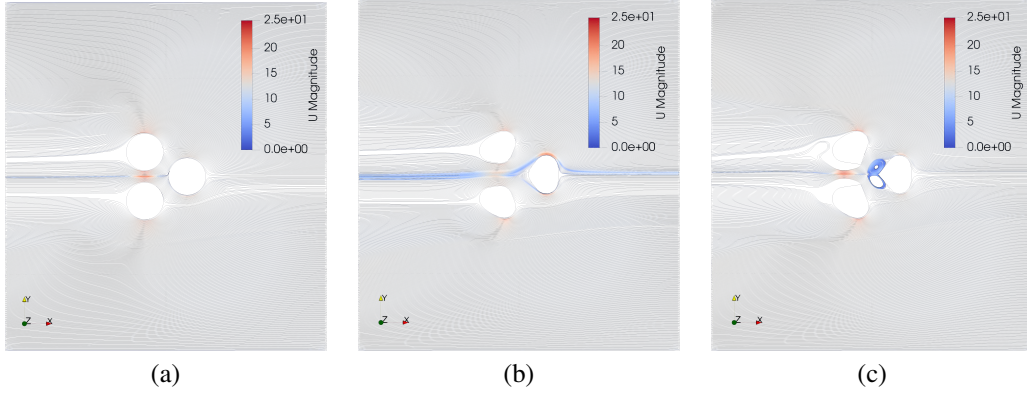(a)   (b)   (c)

Figure 15: 2D CFD results for the cross section shaping (-X wind): (a) circle; (b) triangle with 2 corners fillet and (c) triangle with 3 corners fillet

4.3   Implementation of the 3D model and structural design

The structural members are here defined, imposing as reference the macro-scale parameters included in Tab. 1. Bamboo nodes are terrace level for the outriggers. These structures are designed as a spatial truss made of octahedral modules, forming a large stiff ring in which the central hole has an inner radius of $R_{void} = 10\ m$, and includes the bundled towers. Each internode includes two diagrid triangular modules. A single strip of triangles has been only used for the upper and lower levels. The actions on the building are evaluated as per [40, 41]. The values of the gravitational loads are included in Tab.2 The seismic loading has not been considered in this work since the wind-induced load has greater effect. For the wind loading, the technical document [42] has been additionally referred-to. As reference wind speed, a $100 - years$ return period has been considered, which results in a $v_r = 28.69\ m/s$. The pressure and the forces applied due to wind are schematically represented in fig. 16.

Table 2: Loads acting on the structure

Load	Type	Unit	Value	Load	Type	Unit	Value
Slab package	g_1	kN/m^2	10.00	Live: Residential	q_k	kN/m^2	2.00
Exterior skin package	g_2	kN/m^2	0.50	Live: Office	q_k	kN/m^2	3.00
Interior walls	g_2	kN/m^2	2.00	Live: Hotel	q_k	kN/m^2	2.00
Structural concrete	G_1	kN/m^3	25.00	Live: Commercial	q_k	kN/m^2	4.00
Structural steel	G_1	kN/m^3	78.00	Live: Terraces	q_k	kN/m^2	4.00

The concrete core has been designed to satisfy both structural and architectural demands. Following the tapered profile of each tower, six boxes of reinforced concrete are used; each of them reaches different levels of the building (13th, 35th, 57th, 66th and top floors of the building). Thus, the structure results in a tri-core outrigger with variable cross section. A polar symmetry is preserved in all sections. The core is sized for ULS gravitational-load-combination vertical force and for the ULS wind-prevailing-combination shear force. In this latter case, an unreinforced cross section is considered to be on the safe side. The core thickness and shape are varied at each outrigger. As concrete material the C50/60 class is
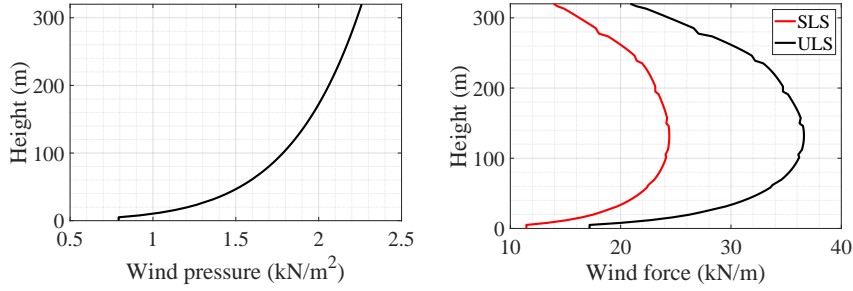
15

Figure 16: Wind pressure and load acting on the building at the Serviceability Limit State (SLS) and Ultimate Limit State (ULS).

employed (see Sec. 4.4).

The diagonal members of the diagrid resist shear forces and the bending moment resulting from wind loads by axial forces in the rods. For sake of redundancy, the inner core contribution to lateral resistance is neglected. The design methodology by Moon et al. [35] has been applied with the purpose of not being thorough, but to provide an approximated solution, which will be the object of further optimization and verification.

In this project, the vertical diagrid module has been dictated by the outrigger spacing. Along the height, one node every two is connected to the outriggers. But in general the diagrid module usually extends over several floors, and the height of each module and consequently the angle of the diagonals is one of the main design parameter. When the building aspect ratio ranges from about 3 to 9, the optimal angle is approximately between 60° and 70° [43]. Moreover, when the building becomes taller, the optimal angle increases because it tends to behave as a beam subjected to bending, so diagonals with a steeper angle resist more effectively to bending moments. The number of triangle edges has been selected to have 70° at the base diameter. The angles and tentative diagrid cross section obtained in this phase are summarized in fig. 17. As material steel S355 is employed (see Sec. 4.4).

The data from the parametric model are transferred to SAP2000 in order to perform FEM analyses by means of the plugin GeometryGym. The mid-plane surfaces of core walls are converted into shell elements, the diagrid axis lines into beam elements. The floors and the outriggers in this phase are modeled as rigid diaphragms on their horizontal planes using a diaphragm constraint. The assignment of materials, cross sections, external loads and their combinations is automatically managed. A preliminary design check is executed before moving on to the diagrid optimization.

Once completed the preliminary design of diagrid and core, a stiffness-driven size optimization is executed with the aim of reducing the diagrid cross-section up to the maximum allowed drift. A more straightforward model has been adopted in the optimization routine with only single tower and translation cantilevers to restore the internal forces provided by the other two towers (fig. 17b). The following routine has been executed for the generative design back and forth between Grasshopper and SAP2000 by means of GeometryGym:

1. Galapagos generates an "individual" by setting the model parameters, which in the present case are the diagrid cross sections;

2. The geometric model related to the specific genome is exported to SAP2000 for a linear analysis, whose result is the displacement at each level;

3. The displacements found are re-imported into Grasshopper, in which the fitness function is evaluated;

4. Galapagos reads the fitness value and starts a new iteration.

The adopted fitting function to be minimized by the solver is expressed as per eq. 4.

$$fitnesss = \sum_{i=1}^{n} \left(\left\| \frac{h_i}{300} - \delta_i \right\| \right) \tag{4}$$

In which δ_i is the level drift, h_i the height of each level, and n is the number of stories. The best result is obtained in at the 12th generation. The summary chart in fig. 18 illustrates the fitness function and the effect on the global drift, which poses a less conservative limitation $\Delta/500$. After the optimization, a significant reduction of the diagrid cross section is obtained, with a material saving of 25.51% (Tab. 3).

16

Table 3: Diagrid optimization: total length, diameter D and weight W of the diagrid before (subscript 0) and after (subscript *opt*) the optimization. The levels are referred to fig. 17.

Level	Tot. length (m)	D_0 (m)	Thickness (m)	D_{opt} (m)	W_0 ($kg \cdot 10^6$)	W_{opt} ($kg \cdot 10^6$)	Variation (%)
M_1	1084.83	2.0	0.08	1.5	4.11	3.04	26.04
M_2	1078.07	2.0	0.08	1.5	4.08	3.02	26.04
M_3	1222.74	2.0	0.08	1.5	4.63	3.43	26.04
M_4	1213.92	2.0	0.08	1.5	4.60	3.40	26.04
M_5	1308.96	2.0	0.08	1.5	4.96	3.67	26.04
M_6	1298.14	2.0	0.07	1.5	4.33	3.20	25.91
M_7	1341.65	2.0	0.07	1.5	4.47	3.31	25.91
M_8	1328.69	1.8	0.07	1.4	3.97	3.05	23.12
M_9	1319.01	1.8	0.07	1.4	3.94	3.03	23.12
M_{10}	1304.44	1.7	0.06	1.2	3.17	2.20	30.49
M_{11}	1255.09	1.4	0.06	1.1	2.49	1.93	22.39
M_{12}	1239.13	1.2	0.06	0.9	2.09	1.54	26.32
M_{13}	1110.90	1.0	0.05	0.7	1.30	0.89	31.58
M_{14}	1089.09	1.0	0.04	0.7	1.03	0.71	31.25
M_{15}	964.17	0.6	0.04	0.6	0.53	0.53	0.00
M_{16}	944.98	0.4	0.03	0.4	0.26	0.26	0.00
Total					49.95	37.21	25.51

4.4 Materials

The materials used in the design and verification of the case study building are included in Tab. 4. Linear elastic behavior is adopted since the analysis goal is not to explore post-elastic capacity of the building. Sizing and optimization consider small displacement theory in order to speed up the process, while the in the design validation large displacement analysis is employed.

Table 4: Material used in the design and verification of the case study building in Pisa

Material	Type	Young's Modulus	Strength	Reference
Steel	S355	$E_s = 210 \, GPa$	$f_{yk} = 355 \, MPa$	[44]
Concrete	C50/60	$E_c = 37 \, GPa$	$f_{ck} = 50 \, MPa$	[45]

5 Design validation and discussion

5.1 Architectural and functional design

Like the greatest part of the modern high-rise buildings, the investigated skyscraper has been supposed to be mixed-use. Thus, with reference to fig. 19, the building has been supplied of:

- residences, located in the tallest floors to reduce the commercial and business interference in the daily residents life;

- offices, located at the middle height;

- an hotel, at the first floors due to the low available space given by the incidence of vertical transportation;

- a commercial area, distributed in the lowest parts as well as in the top of the three towers.

The final design results in a 77-stories mixed-use building, with an available area of $34400 m^2$. The 53% of the floors have been occupied by residences and offices, while 24% of the total space has been assigned to public functions. Each outrigger is characterized by double function: the top level has been designed as a public space connecting the three towers; the low level as a mechanical floor.

For the vertical transportation, elevators and stairs are designed. In particular, the elevator system of each tower is designed to offer a mean waiting time of less than 25 seconds. Each tower has been individually provided by six vertical roads
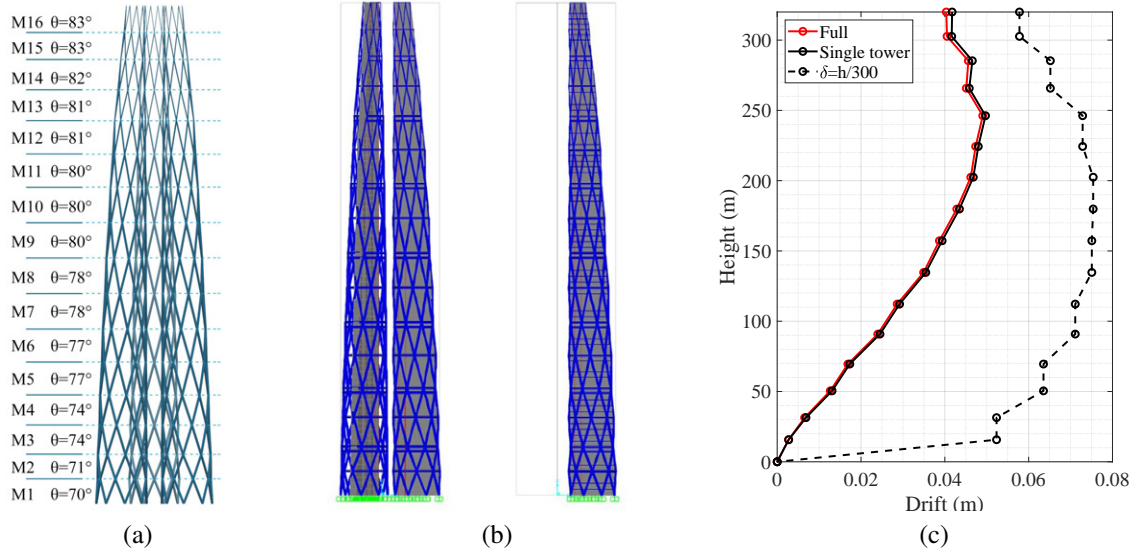
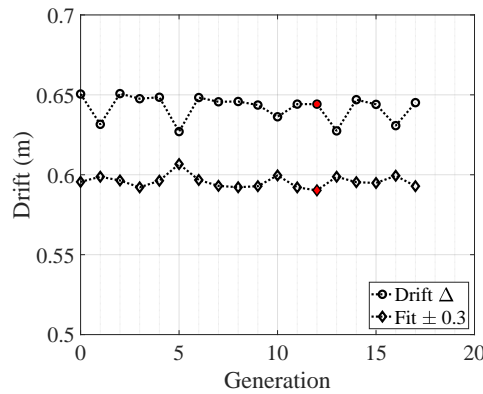Figure 17: Diagrid optimization: (a) angles; (b) full and single-tower simplified models; (c) drift comparison

Figure 18: Size optimization results obtained by means of Galapagos: total drift Δ and fitness function variation.

for a total number of 2 emergency stair ramps and 10 elevators, with a singular maximum capacity of 10 people. All the compartments have been located within the concrete core to guarantee the centrality of the connection hub and to obtain fire-resistance capacity.

The elevators are differentiated for the floor functions they serve according to the scheme of fig. 19. The design takes into account also people flows and their interference. From the safety point of view, the building presents six emergency exit paths, three from the ground to the 57th floor and other three all along the towers. The terraces located at the seven outrigger levels are remarkably strategic because they constitute a safe place where the users can converge in the event of a fire damage in a tower, and easily redirected to the parallel emergency exits. The use of diagrid and core has the advantage of producing free-of-columns floor plans. Three floor plans at different heights are shown in fig. 20.

5.2 Structural verification

Once the main load-bearing elements have been designed and optimized, the focus has been moved to complete the structural design of the outriggers and the VAWT supporting structure and detail the loads on the elements. The outriggers have been explicitly included as a spatial truss, replacing the previous rigid diaphragms. Large displacements are considered in the analysis. The main result is that the building satisfies strength and stiffness requirements posed by the codes either globally and for the single structural element. In order to discuss the assumptions made in the design phase, it is interesting to report a cumulative data in fig. 21, which are the interior forces evaluated at the main sections of the building. Gravitational loading produces axial internal forces that are almost exclusively adsorbed by the core (fig. 21a), therefore

Figure 19: Architectural and functional design: functions allocation and vertical circulation.
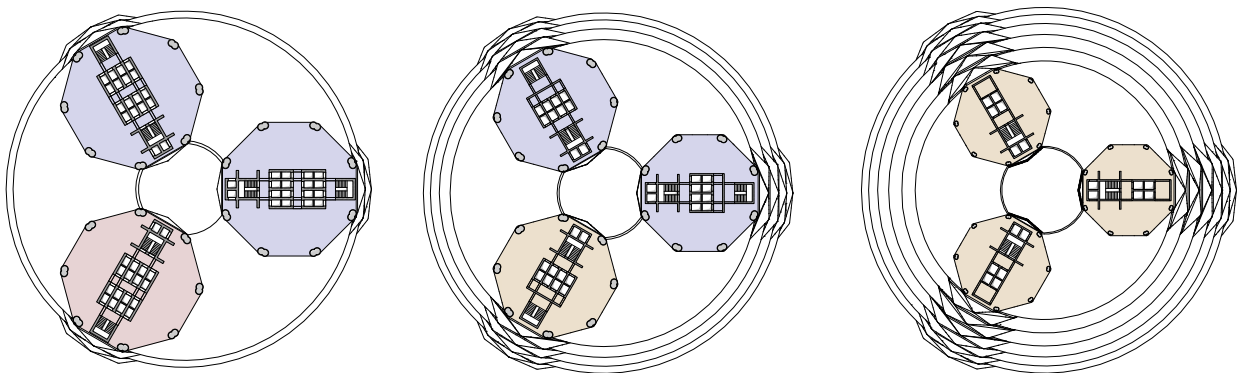

Figure 20: Floor plans at level 69.5 *m*, 157.2 *m* and 246.2 *m* (ref. colors to fig. 19)

the strategy to size the core area to support all vertical loading could be considered acceptable. For the shear (fig. 21b), the concrete core is stiff in the lower levels, while as expected the diagrid provides the prevailing contribution throughout the whole building. Bending is also mostly supported by axial loading on steel outer members; the core results loaded by about one third of the total bending.

To provide discussion on the effectiveness of macro-scale parameter definition (Sec.4.1), the SLS displacements are provided in tab. 5. Additionally, for this purpose another solution is derived by applying a global constraint that fixes the outrigger to move only in-plane. This model has been intended to simulate the shear-only deformation of the building, and its displacements are indicated with the subscript *S*. Instead, the base model has been marked with the subscript *B*. It can be noted that the shear deformation $\delta_{S,x}$ represents on average the 80% of the total deformation $\delta_{B,x}$, so it is the prevailing contribution in the lateral displacement. This data remarks the importance of properly selecting macro-scale parameters to obtain a good shear stiffness. Moreover it appears not wrong to neglect the bending stiffness in the early design phases, as it is done with a simplified single-core model.

The outrigger rotations show a similar trend with respect to the reduced model: the value increases up to the 5th outrigger (approximately 0.6 H) and it remains almost constant, with the only exception of the tip in which there is no outrigger. Nevertheless, also the last internode has a prevailing shear behavior. The vertical displacement associated with the rotations has a profile which has not been predicted by simplified models since it grows approaching the tip instead of lowering. This effect can be ascribed to the optimization of diagrid cross sections.

Even though the building has been conceived using statics, it is important to mention about the dynamic properties of such a new structural system. The FE model to run a modal analysis is obtained from the previous one converting the loads in masses. The periods and participating mass ratios of the first twelve modes are included in tab. 6, the first six modal shapes are shown in fig. 22. It can be observed that the building has a good dynamic stiffness, which is in line with its competitors [46]. The first two modes are translational in the diagonal direction, and their fundamental period is 5.202 s. The third mode is torsional about the vertical axis.

Table 5: Displacements of building for SLS wind prevailing load combination: $\Delta_{-,x}$ is the absolute lateral x displacement; $\delta_{-,x}$ is the relative lateral x displacement; the subscript S denotes the shear only deformation, the B concerns the actual model (so includes also the contribution of bending); $\delta_{adm} = h/300$, $\phi_{B,y}$ is the absolute rotation; $\delta_{B,z}$ is the vertical displacement of the floor associated with that rotation.

Height (m)	$\Delta_{S,x}$ (m)	$\delta_{S,x}$ (m)	$\Delta_{B,x}$ (m)	$\delta_{B,x}$ (m)	δ_{adm} (m)	$\delta_x < \delta_{adm}$	$\phi_{B,y}$ (deg)	Building Diameter (m)	$max(\delta_{B,z})$ (m)
31.4	0.008	0.008	0.0089	0.0089	0.1047	TRUE	0.0078	78.1	0.003
69.5	0.031	0.023	0.0370	0.0281	0.1271	TRUE	0.0306	75.4	0.013
112.2	0.070	0.039	0.0843	0.0473	0.1422	TRUE	0.0508	71.9	0.025
157.2	0.121	0.051	0.1464	0.0620	0.1501	TRUE	0.0640	67.6	0.035
202.5	0.179	0.058	0.2181	0.0718	0.1508	TRUE	0.0712	62.7	0.042
246.2	0.236	0.057	0.2912	0.0731	0.1458	TRUE	0.0725	56.9	0.046
285.3	0.286	0.050	0.3546	0.0635	0.1304	TRUE	0.0756	50.0	0.050
320.0	0.329	0.043	0.4108	0.0562	0.1156	TRUE	0.0842	43.7	0.057

Table 6: Modal analysis: periods and participation mass ratios.

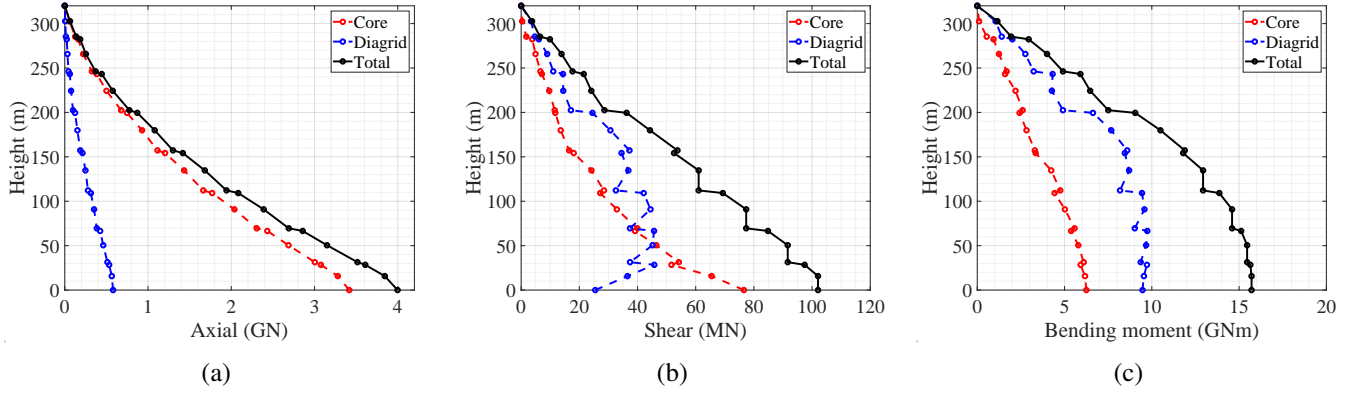| Mode	Period (s)	Partecipating Mass Ratios		
		x	y	z
1	5.202	0.052	0.460	0.000
2	5.202	0.460	0.052	0.000
3	2.423	0.000	0.000	0.000
4	1.622	0.002	0.194	0.000
5	1.622	0.194	0.002	0.000
6	1.261	0.000	0.000	0.000
7	0.850	0.000	0.000	0.000
8	0.843	0.003	0.078	0.000
9	0.843	0.078	0.003	0.000
10	0.666	0.000	0.019	0.000
11	0.666	0.019	0.000	0.000
12	0.598	0.000	0.000	0.000
Sum		0.808	0.808	0.000

Figure 21: Interior forces from the FEM analysis: (a) axial force for ULS gravitational loads; (b) shear and (c) bending moment for the wind-prevailing ULS load combination.
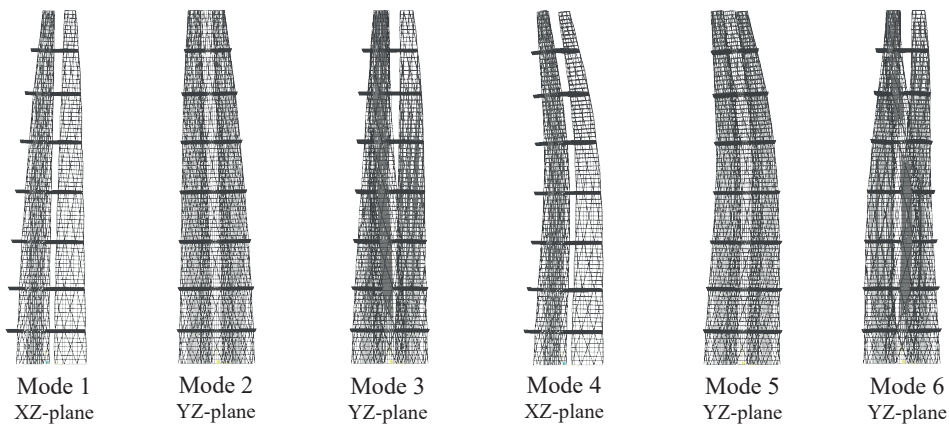

| Mode 1 | Mode 2 | Mode 3 | Mode 4 | Mode 5 | Mode 6 |
| XZ-plane | YZ-plane | YZ-plane | XZ-plane | YZ-plane | YZ-plane |

Figure 22: Modal shapes of the first six modes.

5.3 3D CFD analyses

The 3D CFD analyses have been based on a watertight model of the final geometry. The three towers have been modeled as three smooth elements occupying the gross volume of the diagrids, while the outriggers as flat cylinders (fig. 23). The effects of the surfaces roughness have been neglected since their importance is marginal for the purpose of the analysis. Twelve directions have been investigated according to the wind rose of fig. 23. However, due to symmetry the geometry of the problem is reduced to three cases, in which to apply different boundary conditions:

- +X case, representative of winds from the sectors $30°$, $150°$ and $270°$ (fig. 24a);

- -X case, representative of winds from the sectors $90°$, $210°$ and $330°$ (fig. 24b);

- +Y case, representative of winds from the sectors $0°$, $60°$, $120°$, $180°$, $240°$ and $300°$ (fig. 24c).

The domain of the three cases has been designed as a rectangular bounding box with the long sides oriented as the flow directions. Given D the diameter of the building, the domain longest edge spans from $-12.5\ D$ to $+25\ D$; the smallest from $-10\ D$ to $+10\ D$, the height is 3 times the height of the building. Mesh refinement has been applied at the inlet and at the wake area, and inside the building. The flow has been considered incompressible and in steady state regime, and the RANS method and a Shear-Stress Transport $k - \omega$ turbulence model is adopted. The fluid is atmospheric air with a density $\rho = 1.1965\ kg/m^3$ and a kinematic viscosity of $\nu = 1.5295 x 10^{-5}\ m^2/s$.

Four different boundary conditions have been applied for each case:

- A velocity inlet, identified in the logarithmic wind profile obtained in the statistical site characterization (fig. 23) and applied to the inlet face of the background box.

- A pressure outlet, defined by a Gauge pressure value of zero and assigned to the outlet face of the background box.

- A slip wall condition, assigned to the top and the lateral faces of the background box.

- A no-slip wall condition, assigned to the building geometry and to the lower faces of the background box.
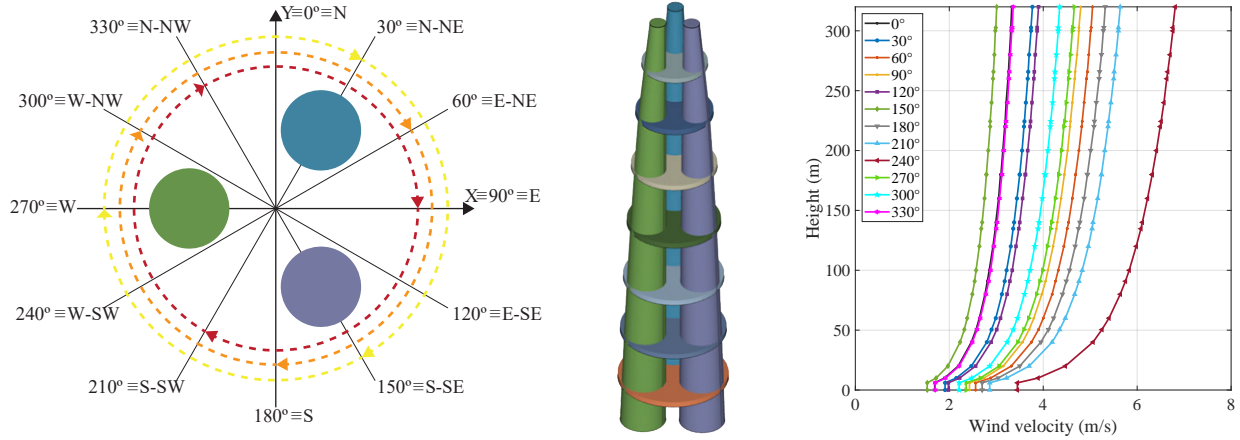

Figure 23: 3D CFD analysis: wind rose, model and adopted wind velocities

The velocity variation between the inlet velocity and the average velocity in the VAWT area for each wind direction is reported in fig. 25. The group of +X case (30°, 150° and 270°) shows an important velocity reduction, which increase if the inlet velocity decreases. This has not been observed in the 2D analysis, indeed the flux deviation involves in this case the third direction and causes a remarkable decrease of kinetic energy. However, this effect is negligible since the -X case characterizes lower wind hours.

For all other cases, the higher is the inlet velocity the greater is the wind flow and the lower is the loss. Concerning the variation with the height, each case (±X, Y) groups curves that present similar tendency. The beneficial shape effect, which increases the velocity inside the building, lowers with the height. This is due to the tapering, which implies cross section reduction and low wind-exposed area. Consequently, a small amount of flow can be directed to the VAWT. However, all curves manifest a flex at the level of the sixth VAWT (266 m) and from that point forward the percentage of velocity increases is higher.

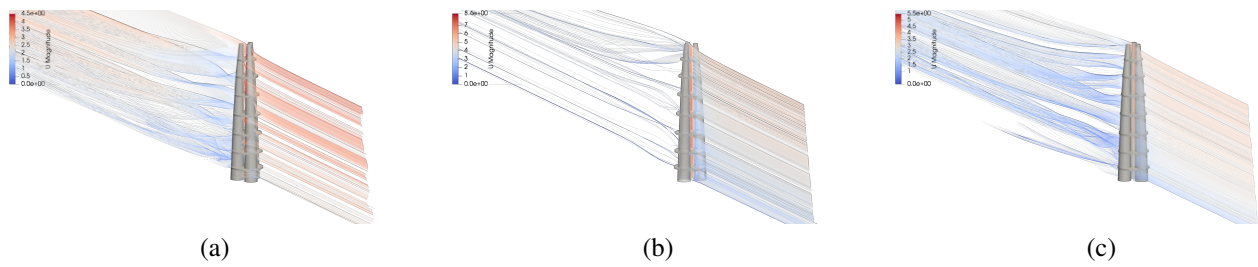(a)   (b)   (c)

Figure 24: Streamline-style representation of the flow in the (a) +X, (b) -X, (c) Y cases.

5.4 Estimation of energy production

The building is equipped with seven VAWTs with features available for common market products. The swept area of each turbine is assumed to be $A = 120 \ m^2$ (12 m height and 10 m diameter) while the cut-in and cut-off speed have been estimated in respectively 2.5 m/s and 22 m/s. The power coefficients have been considered to value $C_P = 0.25$ for a speed range between the cut-in speed and 10 m/s, $C_P = 0.32$ for $10 - 17 \ m/s$ and $C_P = 0.29$ for $17 - 22 \ m/s$. The total power contained in the free wind flow has been obtained for each direction at the height of each turbine by combining the results of the 3D CFD analyses with the data obtained through the wind characterization of the site (fig. 23). These values have been retrieved through the power per unit equation [38]:

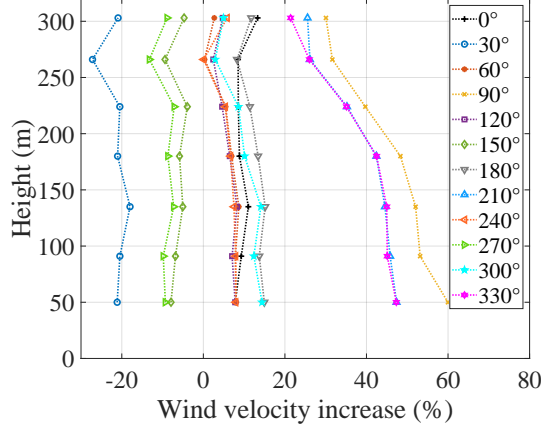$$p_w = 0.5\rho U^3 f(U) \tag{5}$$

22

Figure 25: Wind velocity variation between the inlet velocity and the average velocity in the VAWT area

were ρ is the air density, U is the inlet velocity, $f(U)$ is the frequency of occurrence associated to the same velocity. The power output $P_{t,i}$ of the i-th VAWT has been obtained with the equation:

$$P_{t,i} = \sum_{j=1}^{12} 0.5\rho U_{CFD,j}^3 f(U_j)C_P A \tag{6}$$

where $U_{CFD,j}$ is the CFD-obtained velocity from the j-th direction, $f(U_j)$ is its associated frequency of occurrence. The integration of this equation over the time of one year has then retrieved the annual energy production, resumed in tab. 7. Even if the building obstructs part of the flow directed on the VAWTs, the shape effect is globally beneficial because of the increase of velocity due to the Venturi effect and re-directing of part of the flow due to the shape effect. In fact, comparing the present case with an ideal VAWTs installation in a free flow, the energy gain increases of 108.99 MWh/m^2 with respect to the free flow. In conclusion, with reference to the work [47] the energy gain provided by the VAWTs can be estimated in about the 34% of the total energy consumption of the building. This results in an annual emissions reduction of about 10 $kgCO_2/m^2$.

Table 7: Annual energy production of the VAWTs

Turbine	Location (m)	p_w (W)	P_t (W)	$E_{t,year}$ (MWh)
1	50	463.83	106.68	56.07
2	91	608.12	139.87	73.51
3	135	719.81	165.56	87.02
4	180	809.94	186.29	97.91
5	224	883.72	203.26	106.83
6	266	943.22	216.94	114.02
7	303	990.65	227.85	119.76
Total		5419.28	1246.43	655.13

6 Discussion and conclusions

This work investigates a novel concept for bundled tall buildings that combines multi-core outrigger and diagrid; and proposes a methodology for the shaping through a bamboo biomimetics and for the optimization with respect to the incident wind. This latter point is tackled from the structural viewpoint by designing the stiffness for the wind-induced lateral load, and from the energetic viewpoint by maximizing the wind velocity within the bundles in order to push VAWTs located along the building. The study concludes that the concept is feasible from a theoretical prospective. This is confirmed by the application design case of a tri-bundle 320m-tall building in Pisa, Italy.

The bamboo-based outrigger system presents remarkable advantages in terms of lateral stiffness with respect to an equally-spaced setting. The lateral stiffness of the building demonstrates sensitivity to shear and only to a lesser extent to bending. This effect is caused by the bundling of the cross section. Moreover, the bundled design provides structural and functional redundancy, and produces a Venturi effect, which is beneficial for the VAWTs. The diagrid that enclose each bundle relieves the core from sustaining most of the shear and the bending moment. However, the core constitutes the main bearing element for vertical load.

The aerodynamics of the building favors an increase of velocity within the bundle towers. Distributing several VAWTs along the building height can be stated as a good strategy for what these preliminary analysis have concerned. The cross section shape and the tapering of the building are the main parameters affecting the wind flow. The whole methodology is based on a parametric stream, which gives a complete control of the building components and their models with respect to the goals of each step. Their accuracy is accordingly proportionate, and further detailed analyses have to be developed in the verification phase.

A possible hint for further research is to include a simplified 3D CFD for the cross-section shaping. Indeed, the bi-dimensional wind flux underestimates the losses of velocity incident on the VAWTs. Another point to further develop is the joint optimization of both core and diagrid. This is only apparently a simple problem, and it is strictly related to architectural and functional requirements (i.e. the vertical circulation). Lastly, post-elastic behavior of these new kind of structures has to be characterized.

References

[1] Mahjoub Elnimeiri and Prairna Gupta. Sustainable structure of tall buildings. *The Structural Design of Tall and Special Buildings*, 17(5):881–894, 2008.

[2] Mais Aldwaik and Hojjat Adeli. Advances in optimization of highrise building structures. *Structural and Multidisciplinary Optimization*, 50(6):899–919, 2014.

[3] Dimitris Mavrokapnidis, Chara Ch Mitropoulou, and Nikos D Lagaros. Environmental assessment of cost optimized structural systems in tall buildings. *Journal of Building Engineering*, 24:100730, 2019.

[4] Mir M Ali and Kyoung Sun Moon. Structural developments in tall buildings: current trends and future prospects. *Architectural science review*, 50(3):205–223, 2007.

[5] Yu Zhang and Caitlin Mueller. Shear wall layout optimization for conceptual design of tall buildings. *Engineering Structures*, 140:225 – 240, 2017.

[6] Paolo Foraboschi, Mattia Mercanzin, and Dario Trabucco. Sustainable structural design of tall buildings based on embodied energy. *Energy and Buildings*, 68:254 – 269, 2014.

[7] Xinzheng Lu, Mengke Li, Hong Guan, Xiao Lu, and Lieping Ye. A comparative case study on seismic design of tall RC frame-core-tube structures in China and USA. *The Structural Design of Tall and Special Buildings*, 24(9):687–702, 2015.

[8] Soobum Lee and Andrés Tovar. Outrigger placement in tall buildings using topology optimization. *Engineering structures*, 74:122–129, 2014.

[9] Hyo Seon Park, Eunseok Lee, Se Woon Choi, Byung Kwan Oh, Tongjun Cho, and Yousok Kim. Genetic-algorithm-based minimum weight design of an outrigger system for high-rise buildings. *Engineering Structures*, 117:496 – 505, 2016.

[10] Ying Zhou, Cuiqiang Zhang, and Xilin Lu. An inter-story drift-based parameter analysis of the optimal location of outriggers in tall buildings. *The Structural Design of Tall and Special Buildings*, 25(5):215–231, 2016.

[11] Han-Soo Kim. Optimum design of outriggers in a tall building by alternating nonlinear programming. *Engineering Structures*, 150:91 – 97, 2017.

[12] Chengqing Liu, Qinfeng Li, Zheng Lu, and Handan Wu. A review of the diagrid structural system for tall buildings. *The Structural Design of Tall and Special Buildings*, 27(4):e1445, 2018. e1445 TAL-17-0073.R1.

[13] Chengqing Liu and Dengjia Fang. Robustness analysis of vertical resistance to progressive collapse of diagrid structures in tall buildings. *The Structural Design of Tall and Special Buildings*, 29(13):e1775, 2020. e1775 TAL-19-0311.R1.

[14] Esmaeel Asadi and Hojjat Adeli. Diagrid: An innovative, sustainable, and efficient structural system. *The Structural Design of Tall and Special Buildings*, 26(8):e1358, 2017.

[15] Chengqing Liu and Kaiqiang Ma. Calculation model of the lateral stiffness of high-rise diagrid tube structures based on the modular method. *The Structural Design of Tall and Special Buildings*, 26(4):e1333, 2017. e1333 TAL-15-0159.R2.

[16] Valentina Tomei, Maura Imbimbo, and Elena Mele. Optimization of structural patterns for tall buildings: The case of diagrid. *Engineering Structures*, 171:280–297, 2018.

[17] Giulia Angelucci and Fabrizio Mollaioli. Diagrid structural systems for tall buildings: changing pattern configuration through topological assessments. *The Structural Design of Tall and Special Buildings*, 26(18):e1396, 2017.

[18] Feng Zhao and Chonghou Zhang. Diagonal arrangements of diagrid tube structures for preliminary design. *The Structural Design of Tall and Special Buildings*, 24(3):159–175, 2015.

[19] Simos Gerasimidis, Panos Pantidis, Brendan Knickle, and Kyoung Sun Moon. Diagrid structural system for high-rise buildings: Applications of a simple stiffness-based optimized design. *International Journal of High-Rise Buildings*, 5(4):319–326, 2016.

[20] Giuseppe Lacidogna, Domenico Scaramozzino, and Alberto Carpinteri. A matrix-based method for the structural analysis of diagrid systems. *Engineering Structures*, 193:340 – 352, 2019.

[21] Maryam Asghari Mooneghi and Ramtin Kargarmoakhar. Aerodynamic mitigation and shape optimization of buildings. *Journal of building engineering*, 6:225–235, 2016.

[22] Dong-Xue Zhao and Bao-Jie He. Effects of architectural shapes on surface wind pressure distribution: case studies of oval-shaped tall buildings. *Journal of Building Engineering*, 12:219–228, 2017.

[23] Fan-Qin Meng, Bao-Jie He, Jin Zhu, Dong-Xue Zhao, Amos Darko, and Zi-Qi Zhao. Sensitivity analysis of wind pressure coefficients on caarc standard tall buildings in cfd simulations. *Journal of Building Engineering*, 16:146–158, 2018.

[24] CM Chan, MF Huang, and Kenny CS Kwok. Integrated wind load analysis and stiffness optimization of tall buildings with 3d modes. *Engineering structures*, 32(5):1252–1261, 2010.

[25] Ahmed Elshaer, Girma Bitsuamlak, and Ashraf El Damatty. Enhancing wind performance of tall buildings using corner aerodynamic optimization. *Engineering Structures*, 136:133–148, 2017.

[26] Richard F Smith and Shaun Killa. Bahrain World Trade Center (BWTC): the first large-scale integration of wind turbines in a building. *The structural design of tall and special buildings*, 16(4):429–439, 2007.

[27] Q.S. Li, Z.R. Shu, and F.B. Chen. Performance assessment of tall building-integrated wind turbines for power generation. *Applied Energy*, 165:777 – 788, 2016.

[28] Dennis Poon, Shaw-song Shieh, LM Joseph, and C Chang. Structural design of taipei 101, the world's tallest building. In *Proceedings of the CTBUH 2004 Seoul Conference, Seoul, Korea*, pages 271–278, 2004.

[29] Mark Sarkisian. *Designing tall buildings: structure as architecture*. Routledge, 2016.

[30] Göran Pohl and Werner Nachtigall. *Biomimetics for Architecture & Design: Nature-Analogies-Technology*. Springer, 2015.

[31] Jules JA Janssen. *Designing and building with bamboo*. International Network for Bamboo and Rattan Netherlands, 2000.

[32] Robert McNeel and Associates. Grasshopper generative modeling for Rhino. *Computer software, http://www. grasshopper3d. com*, 2018.

[33] OpenCFD Ltd (ESI Group). OpenFOAM® Documentation. *Computer software documentation, http://www.openfoam.com*, 2019.

[34] Ladybug Tools LLC. Butterfly primer. *Computer software documentation, https://docs.ladybug.tools/butterfly-primer/*, 2019.

[35] Kyoung-Sun Moon, Jerome J Connor, and John E Fernandez. Diagrid structural systems for tall buildings: characteristics and methodology for preliminary design. *The structural design of tall and special buildings*, 16(2):205–230, 2007.

[36] Geometry Gym Pty Ltd. Geometry Gym Technical. *Computer software documentation, https://technical.geometrygym.com/*, 2019.

[37] CSI. SAP2000: CSI Analysis Reference Manual. *Computer software documentation, https://wiki.csiamerica.com/*, 2019.

[38] Ib Troen and Erik Lundtang Petersen. *European Wind Atlas*. Risø National Laboratory, 1989.

[39] SimScale GmbH. SimScale Documentation. *Computer software documentation, https://www.simscale.com/docs/*, 2019.

[40] CEN. *EN 1990:2002 - Eurocode - Basis of structural design*. European Committee For Standardization, 2005.

[41] MIT. *NTC18 - Norme tecniche per le costruzioni*. Ministro delle infrastrutture e dei trasporti, 2018.

[42] CNR. *Istruzioniper la valutazione delle azioni e degli effettidel vento sulle costruzioni*. Consiglio Nazionale delle Ricerche CNR-DT 207/2008, 2008.

[43] Jinkoo Kim and Young-Ho Lee. Seismic performance evaluation of diagrid system buildings. *The Structural design of tall and special buildings*, 21(10):736–749, 2012.

[44] CEN. *EN 1993-1-1 - Eurocode 3: Design of steel structures - Part 1-1: General rulesand rules for buildings* . European Committee For Standardization, 2005.

[45] CEN. *EN 1992-1-1 Eurocode 2: Design of concretestructures - Part 1-1: General rules and rules for buildings*. European Committee For Standardization, 2004.

[46] Peifu Xu, Congzhen Xiao, and Jianhui Li. Research on relationship between natural vibration periods and structural heights for high-rise buildings and its reference range in china. *International Journal of High-Rise Buildings*, 3(1):49–64, 2014.

[47] Daniel Godoy-Shimizu, Philip Steadman, Ian Hamilton, Michael Donn, Stephen Evans, Graciela Moreno, and Homeira Shayesteh. Energy use and height in office buildings. *Building Research & Information*, 46(8):845–863, 2018.